Cracking of porcelain coatings bonded to metal substrates of different modulus and hardness

Hong Zhao,[a] Xiaozhi Hu, and Mark B. Bush
Department of Mechanical and Materials Engineering, The University of Western Australia, Nedlands, WA 6907, Australia

Brian R. Lawn
Materials Science and Engineering Laboratory, National Institute of Standards and Technology, Gaithersburg, Maryland 20899

(Received 13 December 2000; accepted 1 March 2001)

A preceding study of contact damage in a bilayer system consisting of a porcelain coating on a stiff Pd-alloy substrate is here expanded to investigate the role of substrate modulus and hardness. Bilayers are made by fusing the same dental porcelain onto Co-, Pd-, and Au-alloy metal bases. Indentations are made on the porcelain surfaces using spheres of radii 2.38 and 3.98 mm. Critical loads to initiate cone fracture at the top surface of the porcelain and yield in the substrate below the contact are measured as a function of porcelain thickness. Radial cracks form at the lower surface of the coating once the substrate yield is well developed. By virtue of its controlling role in the metal yield process, substrate hardness is revealed to be a key material parameter—substrate modulus plays a secondary role. A simple elasticity-based analysis for predetermining critical loads for a given brittle/plastic bilayer system is presented.

I. INTRODUCTION

Ceramic coatings on metal substrates are of technological importance in engineering and biomechanical applications requiring high-wear resistance and mechanical, thermal, or chemical insulation. Dentistry, where ceramic coatings on metal underlayers form the basis of traditional crown and bridge design,[1,2] is an illustrative case in point—a porcelain coating layer provides wear resistance and aesthetics, a metal core provides mechanical support for the porcelain, and the composite ceramic–metal bilayer provides protection for the inner tooth dentin structure. Such coating/substrate structures tend to be highly vulnerable to fracture in concentrated loads,[3–9] raising the issue of the most desirable material properties for ensuring crack-free structures.

In a recent study of Hertzian indentation of a brittle porcelain coating on a Pd-alloy substrate[10] the critical role of the metal substrate in the fracture of the ceramic overlayer was demonstrated. The metal may indeed provide a relatively stiff support, yet may actually promote certain kinds of fracture in the coating by yielding beneath the contact—the coating then flexes like an axisymmetric plate on a compliant foundation, initiating radial cracks at the lower surface (i.e., at the coating/substrate interfaces)—these cracks subsequently spread subsurface in elongate fashion on median planes containing the load axis. Radial cracks are dangerous because they can grow at relatively low loads, and can be difficult to detect in opaque materials. They are considered to be a primary source of failure in dental crowns.[2] These cracks are in addition to the conventional cone cracks that initiate from the top coating surface in the Hertzian contact zone. Cone cracks tend to form in thicker coatings, radial cracks in thinner coatings. This same cone–radial crack competition is observed in coatings on low modulus (polymeric) substrates[11] although there the thin plate flexure is due to elastic compliance rather than to yield of the substrate. Interestingly, delamination is not a prevalent mode of first fracture in these systems.

In this paper we continue from our preceding study[10] and investigate the role of different metal substrate properties in the fracture of low-modulus (porcelain) coatings in concentrated loading at the top surface, by investigating three metal alloys. Whereas the systems under study comprise dental materials, the results have a broad generality. Specifically, we determine the critical loads to produce controlling damage modes, cracking in the coating, and yield in the substrate. Substrate yield and ensuing radial cracking in the coating are observed using

[a]Guest scientist at the National Institute of Standards and Technology.

section experiments. We demonstrate that critical load trends for top surface cone cracks alone can provide valuable indicators as to the onset of subsurface radial cracks, without the need for (time-consuming) sectioning. An elastic stress analysis is used to derive working relations for the critical conditions for the onset of both fracture and yield modes. These relations account for the data trends, and accordingly provide basic guidelines for ceramic/metal bilayer design. We show that high hardness is the primary substrate property for resistance to radial fracture in low-modulus brittle coating systems. Increasing substrate modulus can actually be counterproductive, by (weakly) enhancing the fracture modes.

II. MATERIALS AND METHODS

A. Experiments

A schematic of the test system is shown in Fig. 1. A bilayer consisting of a hard, brittle coating of thickness d fused to a stiff but soft, thick metal alloy substrate is subjected to indentation at the top surface with a sphere of radius r at load P. Damage modes considered are cone (C) and radial (R) cracks in the coating, and yield (Y) zones in the substrate.

Materials used in the present study are those commonly used in the fabrication of dental crowns: for the coatings, a feldspathic porcelain; for the metal substrates, cobalt (Co-), palladium (Pd-) (from the preceding study [10]) and gold (Au-) alloys. Compositions, suppliers, and basic material properties are listed in Table I. For each material, Young's modulus was measured using a sonic method (Grindosonic MK5, J.W. Lemmens Inc., St. Louis, MO). Indentation hardness H (load/projected area of impression)[12] was measured from the diameter of Vickers indentations (Zwick 3212, Zwick USA, Kennesaw, GA). In accordance with dental crown preparation protocols, thermal expansion mismatch between the porcelain and each of the metals was not high, $\Delta\alpha < 1 \times 10^{-6}\ ^{\circ}C^{-1}$, so that residual stresses may be neglected.[13,14] Note that Co- and Au-alloys fall on either side of Pd-alloy in modulus and hardness, expanding the range of metal substrate properties covered in the preceding study.[10] Note also that all the metals have higher elastic modulus E than porcelain, but substantially lower hardness H.

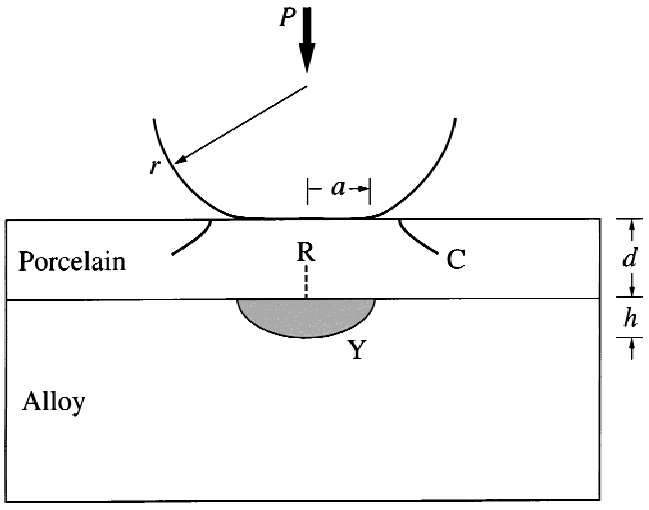

FIG. 1. Schematic drawing of porcelain/metal bilayer, coating thickness d, showing contact with sphere of radius r at load P, with resultant contact radius a. Above critical loads, contact produces transverse cone cracks (C) and radial cracks (R) in coating; and yield zone (Y), depth h, in substrate.

Porcelain/metal bilayers were prepared according to dental manufacturer specifications. The metals were obtained as pellets and cast into substrate blocks 20 × 15 × 3 mm from the melt. Top and bottom surfaces were ground and polished flat and parallel. The Au-alloy specimens were degassed at 980 °C, to avoid bubble formation at the porcelain/metal interface. All metal surfaces were sandblasted to provide adhesion to the ensuing porcelain veneer. Porcelain was then applied as a slip onto the metal base, in layers of 300 μm maximum thickness at a time. A firing cycle to 900 °C was used to sinter each porcelain layer sequentially, to a total thickness of approximately 1 mm. The top porcelain surfaces were then ground and final polished with 1 μm diamond paste to thicknesses in the range $d = 0.1$–1 mm.

Indentation tests were made on the top surfaces of the porcelain/metal bilayer specimens, using tungsten carbide (WC) spheres of radius $r = 2.38$ and 3.98 mm (i.e., in a range applicable to cuspal radii in dental restorations).[15] The indenter was mounted in the crosshead of an Instron testing machine (Instron 1122, Canton, MA), and driven at a constant crosshead speed 0.2 mm · min^{-1}. All indentation tests were carried out in air.

Bonded-interface bilayer specimens[16,17] were used to observe subsurface damage modes. Blocks were cut into halves parallel to their long dimensions, polished at their cut sides, and glued together again with adhesive (Loctite Corp., Newington, CT). Top surfaces were then polished to ensure flatness. Indentations were made along the trace of the interface at the top surface. The indented specimens were then immersed in acetone to dissolve the adhesive and separate the opposing halves. After cleaning, these were viewed in an optical microscope using Nomarski illumination. Porcelain thicknesses were measured from these sections.

Critical loads for the onset of damage were measured by post-contact observation of indented bilayer specimens.[15] Cone crack initiation in the porcelain was measured on (non-sectioned) bilayer specimens by making series of indentations at ever-increasing loads in lines along the top porcelain surfaces—the value P_C was then determined as the load range over which the surface ring crack first appeared as a small arc immediately outside

TABLE I. Materials used in this study.[a]

Material	Composition (wt %)	Brand name supplier	Young's modulus E (GPa)	Hardness[b] H (GPa)	Thermal expansion (10^{-6} °C^{-1})
Veneer		Vita Omega 900	66	6.2	13–14
Porcelain[c]		Vita Zahnfabrik Bad Säckingen Germany			
Substrate					
Co-alloy	Co 55% Cr 25% W 10% Other metals 10%	Novarex Jeneric/Pentron, Inc. Wallingford, CT	231	3.0	14.1
Pd-alloy	Pd 81.5% Sn 14.5% Ga 3.5% Other metals 0.5%	Argipal Argen Precious Metals San Diego, CA	126	2.0	14.1
Au-alloy	Au 88% Pt 9% In 1.5% Other metals 1.5%	Argident 88 Argen Precious Metals San Diego, CA	92	1.2	14.5

[a]Information on product names and suppliers in this paper is not to imply endorsement by NIST.
[b]Hardness H = load/projected area of Vickers indentation = $1.078H_V$.
[c]Strength of porcelain σ_F = 130 MPa ± 20 N.

the contact and subsequently completed itself in a full trace around the contact circle. Uncertainties in P_C from these measurements are of order ±10–20 N. The critical value P_Y for yield in the Pd-alloy substrate was determined by measuring the depths h (Fig. 1) at given loads P directly from bonded-interface section views of the plastic zones, and extrapolating the data back to zero depth.[10] These extrapolations are somewhat subjective, and the uncertainty in P_Y is estimated at ±40–50 N. Values of P_R were not measured directly, but it was confirmed in all cases that radial cracks never initiated until the yield zone in the support metal was well-developed.[10]

B. Stress analysis

A simple software package (Elastica, Technische Universität Chemnitz, Chemnitz, Germany) was used to compute stresses in the bilayers—principal tensile stresses σ_1 in the porcelain coatings and von Mises shear stresses $\sigma_S = \{\frac{1}{2}[(\sigma_1 - \sigma_2)^2 + (\sigma_2 - \sigma_3)^2 + (\sigma_3 - \sigma_1)^2]\}^{1/2}$ in metal-alloy substrates. This algorithm is based on explicit analytical solutions of the elasticity equations for a bilayer in loading by a sphere[18]—it thereby requires far less computer time than traditional finite element algorithms (typically seconds rather than hours). Although confined to elastic fields, the algorithm remains valid up to the point of first fracture or plastic deformation, and so provides the basis for evaluating critical loads P_C and P_Y for coating cracking and substrate yield, respectively.

Modulus and hardness parameters for input into the algorithm are taken from Table I. Young's modulus E is the principal elastic constant. (Generic values are used for Poisson's ratio: $\nu = 0.25$ for the ceramic coatings and $\nu = 0.35$ for the metal substrates. Shear stresses are not sensitive to ν although tensile stresses may be).[19] Hardness H is used to provide estimates of the yield stresses of the metals, $Y = H/3$,[12] for determination of P_Y.

III. RESULTS

A. Experimental data

Figure 2 shows half-surface and side-section micrographs of damage in porcelain/Co-alloy, porcelain/Pd-alloy, and porcelain/Au-alloy bonded-interface bilayer specimens, for a fixed load $P = 500$ N and coating thickness $d = 300$ μm. The indentation load in each case is well above the critical level required to produce damage, but show differences in the damage patterns most clearly. Most evident is the systematic increase in degree of substrate yield from Co- to Pd- to Au-alloy substrate, i.e., with decreasing hardness and modulus (Table I). In the Pd- and Au-alloy the yield zones extend laterally well beyond the indentation contact diameter, indicating that the substrate is bearing the bulk of the applied load. Radial cracks extending upward from the coating/substrate interface develop as the yield becomes more extensive, consistent with enhanced flexure of the plate-like porcelain coating. On the other hand, the cone-crack patterns on the top half-surfaces show relatively little variation from bilayer-to-bilayer. No delaminations are observed in Fig. 2 (although they have been demonstrated in the preceding study to occur at higher loads in specimens with thinner coatings).[10]

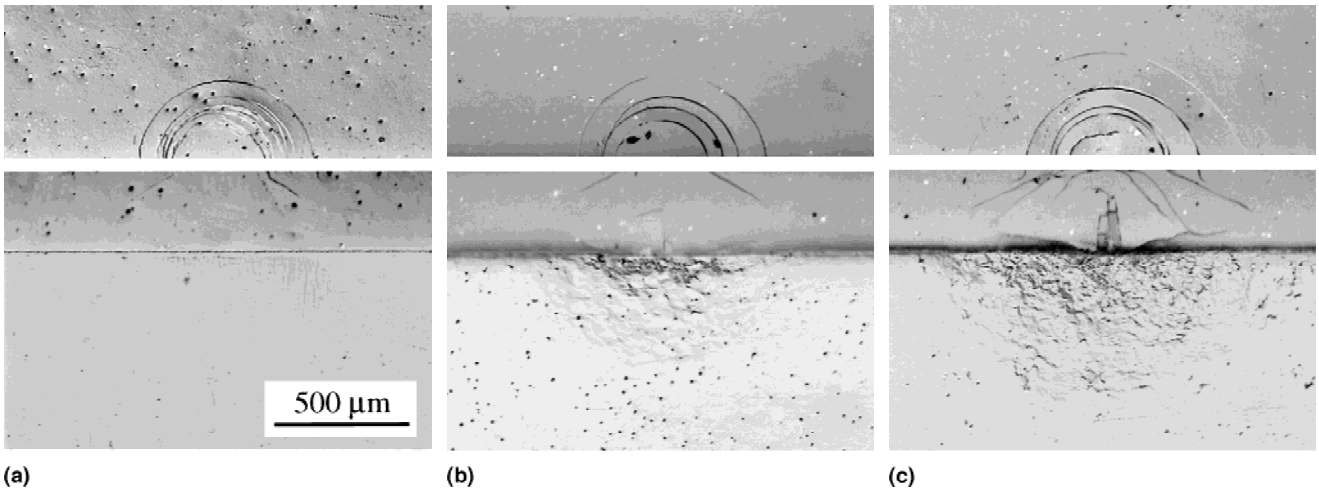

FIG. 2. Half-surface and side view micrographs comparing damage in porcelain/metal bilayers at load $P = 500$ N and coating thickness $d = 300$ μm, substrate (a) Co-alloy, (b,) Pd-alloy, and (c) Au-alloy, WC sphere radius $r = 2.38$ mm.

Critical load data for cone cracking and yield are plotted as a function of porcelain thickness d in Figs. 3–5 for bilayers with Co-, Pd-, and Au-alloy substrates, P_C for sphere radii $r = 2.38$ and 3.98 mm, and P_Y for sphere radius $r = 2.38$. Data points with uncertainty bounds are experimental determinations. Solid curves are stress analysis calculations (next subsection). The P_C data initially show a slight decline with diminishing d, most pronounced for the high-modulus Co-alloy substrates, with a rising then falling "tail" in the region $P_Y < P_C$ at low d. The P_Y data, on the other hand, increase monotonically with d, intersecting the P_C data sets at some characteristic thickness d, dependent on substrate material and sphere radius r. Values of P_R are not measured directly in our experiments but, since $P_R > P_Y$ in these bilayers, we can conclude that radial cracking occurs somewhere in the $P_C(d)$ tail referred to above.

B. Stress analysis

Figure 6 shows calculated distributions of relevant stress components in the bilayers for coating thickness $d = 0.3$ mm at two contact loads $P = 100$ N (corresponding to near-threshold conditions for damage) and 500 N (corresponding to the conditions in Fig. 2), at designated sphere radii. (We emphasize that these distributions are computed as though the stress field remains elastic at all loads.) From such distributions as these we can evaluate critical loads P_C and P_Y for comparison with the experimental data in Figs. 3–5.

Cone cracks. Figure 6(a) plots tensile stress σ_1 as a function of radial coordinate from the indentation center at the top coating surface. The stiffer substrates lead to a small but real enhancement of σ_1 just outside the contact where the cone cracks initiate. The fact that the differences between the three sets of curves are small demonstrates a relatively minor role of substrate modulus on the near-surface Hertzian contact field. Note that the peak stresses are not linear in P, and are in fact closer to a dependence $\sigma_1 \propto P^{1/3}$ characteristic of Hertzian contacts on monoliths.[19,20] The σ_1 peak stress levels are well in excess of the four-point bend strength $\sigma_F = 130$ MPa for our porcelain (dashed line), even at the lower load $P = 100$ N close to the critical value P_C for the $r = 2.38$ mm data in Figs. 3–5. This simply confirms the well-documented Hertzian fracture behavior in monoliths: that cone cracks initiate in a rapidly diminishing σ_1 field below the contact surface, so that a higher surface stress level is required to initiate full cone fracture.[20–22]

Nevertheless, at least to first approximation, we may argue that the critical load for initiation in different porcelain coatings should scale in (inverse) proportion to the σ_1 peak value. Thus, for coatings of modulus E_c and toughness T_c we may accommodate the effect of coating thickness and modulus mismatch into the well-known critical load relation for monoliths ("Auerbach's" law)[20–22]

$$P_C = AT_c^2 r/E_c \quad , \tag{1}$$

by writing $A = A(d/r, E_c/E_s)$. This relation is contingent on the existence of sufficiently large flaws to ensure initial stability of the surface ring crack prior to instability. (In the present case, this is guaranteed by the presence of natural internal flaws, crystalline inclusions, and voids, in the porcelain microstructure.[15]) To evaluate $P_C(d/r, E_c/E_s)$, we first calculate the peak value of σ_1 for monolithic porcelain ($d/r \to \infty$, $E_c/E_s = 1$) corresponding to the critical load P_0 at $r = 2.38$ and 3.98 mm (for monolithic porcelain, $P_0/r = 54$ N/mm over the range of r covered).[10] Then we determine the critical load P_C to attain this same peak stress level for any specified values of d/r and E_c/E_s. The resulting functions are those plotted as the solid $P_C(d)$ curves in Figs. 3–5.

Substrate yield. Figure 6(b) plots the von Mises stress $\sigma_S = \{\frac{1}{2}[(\sigma_1 - \sigma_2)^2 + (\sigma_2 - \sigma_3)^2 + (\sigma_3 - \sigma_1)^2]\}^{1/2}$ as a function of axial coordinate along the contact axis measured from the indentation center at the coating top surface. Again, the stiffer substrates enhance the stress level, but the differences between substrates are slight, indicating a minor role of elastic mismatch. In this case the stress levels in the substrate are more closely in proportion to the contact load, indicating that the surface contact conditions are less important in the far-field stress distributions. Included in Fig. 6(b) are yield stress levels $Y = H/3$ for each material (dashed lines). These latter indicate that yield stresses in the softer substrates are likely to be attained at lower contact loads; and certainly before yield in the porcelain (even allowing that the shear stresses in the coating layer are considerably higher). These observations are qualitatively consistent with the relative degrees of substrate yield in the micrographs of Fig. 2.

Accordingly, we use the elastic calculations to estimate the conditions for onset of first yield, as follows. Since the substrate stresses must be insensitive to contact area (St. Venant's principle),[23] we assume an artificially small value $r = 0.1$ mm for the sphere radius in the calculations ("point-load" limit, $r \ll d$). In this approximation, the von Mises stresses at any point in a given substrate may be expected to scale as $\sigma_S \propto P/d^2$, consistent with a Boussinesq concentrated-force field.[23] Invoking the yield condition $P = P_Y$ at $\sigma_S = Y = H/3$, we obtain a relation of the form

$$P_Y = GH_s d^2 \quad , \tag{2}$$

with $G = G(E_c/E_s)$ a modulus mismatch factor. [Strictly, we should include an intercept load $P_{Y0} = (0.37\pi H_s)^3(4k/3E_c)^2 r^2$ on the right-hand-side of Eq. (2), to allow for nonzero yield in the substrate monolith at $d = 0$.[20] However, P_{Y0} is relatively small in the cases considered here, and may be ignored to first approximation.] A numerical evaluation of $G(E_c/E_s)$ (for $\nu_c = 0.25$ and $\nu_s = 0.35$) is shown in Fig. 7, empirically fitted by the linear relation

$$G = \alpha + \beta E_c/E_s \quad , \tag{3}$$

with $\alpha = 0.566$ and $\beta = 0.166$. Note that G decreases as E_c/E_s decreases, but becomes slowly varying at $E_c \ll E_s$,

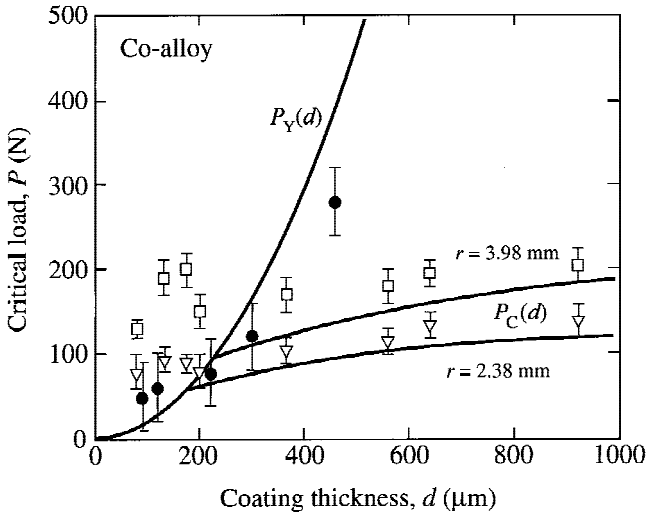

FIG. 3. Critical loads versus porcelain coating thickness d, on Co-alloy substrate, P_C for WC sphere radius $r = 2.38$ and 3.98 mm and P_Y for WC sphere radius $r = 2.38$ mm. Error bars are uncertainty bounds. Solid curves are from elastic field analysis.

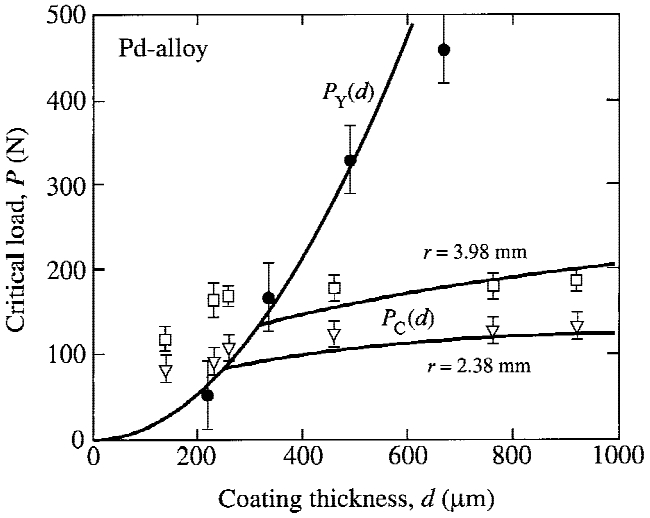

FIG. 4. Critical loads versus porcelain coating thickness d, on Pd-alloy substrate, P_C for WC sphere radius $r = 2.38$ and 3.98 mm and P_Y for WC sphere radius $r = 2.38$ mm. Error bars are uncertainty bounds. Solid curves are from elastic field analysis.

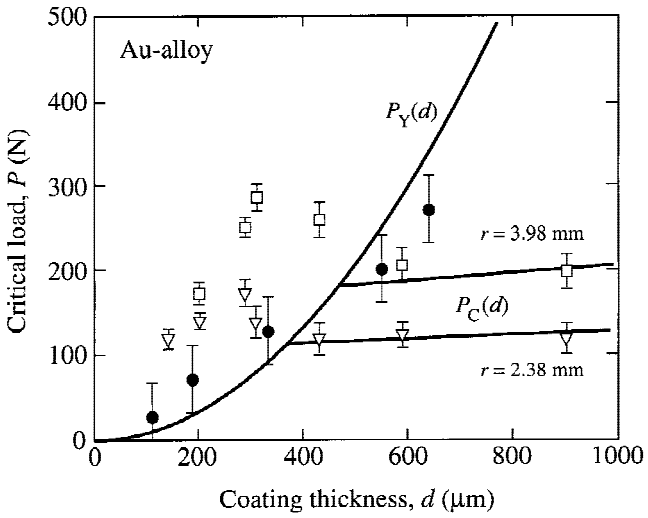

FIG. 5. Critical loads versus porcelain coating thickness d, on Au-alloy substrate, P_C for WC sphere radius $r = 2.38$ and 3.98 mm and P_Y for WC sphere radius $r = 2.38$ mm. Error bars are uncertainty bounds. Solid curves are from elastic field analysis.

with a minimum value $G = 0.566$ for an ideally rigid substrate ($E_c/E_s = 0$). Plots of $P_Y(d)$ from Eqs. (2) and (3) are included as the solid curves in Figs. 3–5.

IV. DISCUSSION

We have examined fracture and deformation modes in bilayers of porcelain coatings on selected metal-alloy substrates in contact loading. These modes are the same as those identified in our preceding study on a single metal (Pd-alloy) substrate:[10] cone cracking in the top coating surface; plasticity in the substrate followed by radial cracking in the bottom coating surface. Substrate plasticity greatly enhances local coating deflection and thereby imposes a flexural tensile stress at the lower coating surface, resulting in radial fracture (while simultaneously imposing a compressive stress at the upper surface, inhibiting cone fracture). Radial cracks are especially deleterious in thinner coatings—they are believed to be a dominant mode of failure in dental crowns.[2] Since yield is a necessary precursor to radial cracking in such systems ($P_Y < P_R$), substrate hardness emerges as a key material property.

The relations in Eqs. (1)–(3) provide us with a simple basis for quantifying these observations, and thence for designing ceramic/metal bilayers against contact fracture. In terms of Figs. 3–5, the key is to operate below the envelope of appropriate $P_C(d)$ and $P_Y(d)$ curves—note that remaining below the $P_Y(d)$ curve is a conservative condition for guarding against radial cracking. It is useful to consider this requirement in relation to a nominal design load P_* (e.g., bearing load in engine applications, or biting force in dental function). Then Eqs. (1) and (2) yield, respectively,

$$d_* = (P_*/GH_s)^{1/2} \quad , \tag{4a}$$

$$r_* = P_* E_c/AT_c^2 \quad , \tag{4b}$$

recalling that $G = G(E_c/E_s)$ and $A = A(d/r, E_c/E_s)$ are relatively slowly varying functions for brittle coating on stiff substrates (i.e., for $E_c < E_s$). Hence the condition for avoiding yield (and radial cracking) is that $d > d_*$ (maintain sufficient coating thickness); and the condition for averting cone cracking is that $r > r_*$ (avoid sharp contacts). The utility of Eq. (4) facilitates simple predictions from basic material parameters (modulus, hardness, toughness)—evaluations of the quantities $G = G(E_c/E_s)$ and $A = A(d/r, E_c/E_s)$, respectively, from Eq. (3)and experimental determinations of P_C on monolith coating

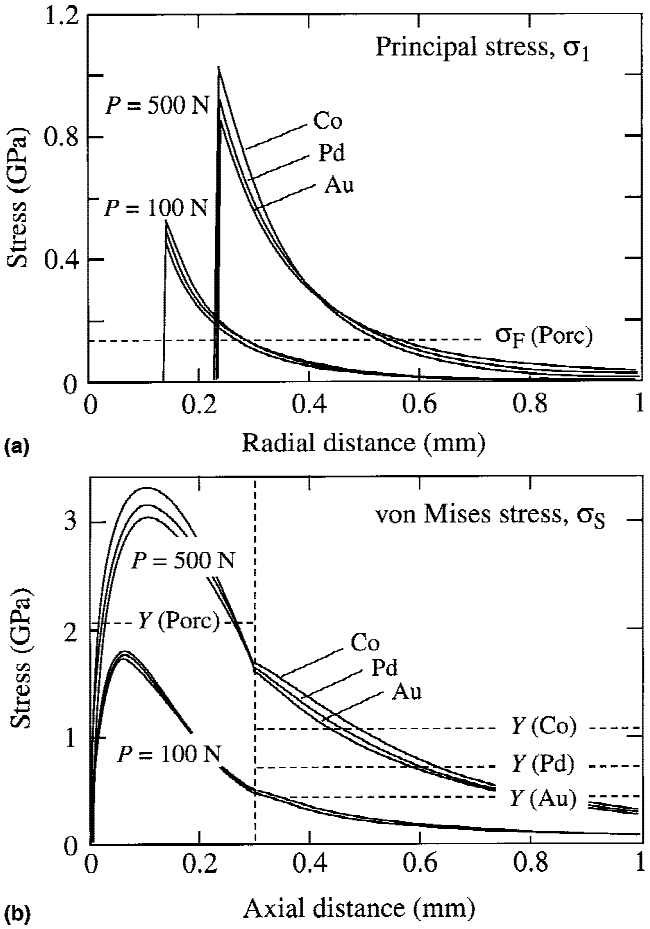

FIG. 6. Plots of relevant stresses in porcelain/metal-alloy bilayers, porcelain thickness $d = 0.3$ mm, at WC sphere loads $P = 100$ and 500 N: (a) principal tensile σ_1 along radial coordinate in top coating surface for radius $r = 2.38$ mm; and (b) von Mises stress $\sigma_S = \{\frac{1}{2}[(\sigma_1 - \sigma_2)^2 + (\sigma_2 - \sigma_3)^2 + (\sigma_3 - \sigma_1)^2]\}^{1/2}$ along axial coordinate for $r = 0.1$ mm ("point load"). Horizontal dashed lines indicate strengths σ_F and yield stresses Y of materials.

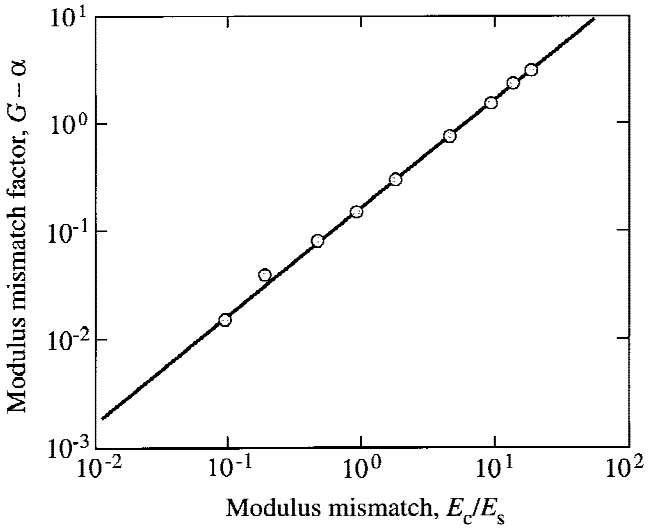

FIG. 7. Plot of $G - \alpha$ versus E_c/E_s, plotted logarithmically to highlight results in the region $E_c/E_s < 1$ of interest here. Data points are analytical determinations for $r = 0.1$ mm (concentrated load), with $\nu = 0.25$ for ceramic coating and $\nu = 0.35$ for metal substrate.

materials (assuming A approximately constant) then enable first-approximation estimates, without the need for extensive and time-consuming (e.g., bonded-interface) measurements.

The relations in Eq. (4) clarify the important material properties. To minimize substrate yield, the primary requirement is for a high substrate hardness H_s in Eq. (4a), as foreshadowed above. A high substrate modulus E_s may be counterproductive because it diminishes G in Eq. (3), although the slow variation of G at low E_c/E_s renders this a secondary consideration. To minimize cone cracking, the primary requirement is for a high coating toughness T_c in Eq. (4b). Again, the role of modulus parameters (E_c/E_s, via A, and E_c) is somewhat secondary.

It is pertinent to remark on the critical conditions for radial cracking. We have noted that yield is an essential precursor to radial cracking ($P_Y < P_R$) in our stiff, metal-based substrate systems ($E_c/E_s < 1$). We have indicated that radial cracking occurs within the "tails" of the $P_C(d)$ data, to the left of the $P_Y(d)$ curves, in Figs. 3–5. Analogous bilayer studies on brittle coatings bonded to very low modulus polymeric substrates[11,24] show even more pronounced tails—in those studies the association of radial cracking with such tails, signaling a transition from Hertzian-dominated to flexure-dominated stress fields, is clearly demonstrated. In the latter region, the strength of the undersurface of the flexed coating layer becomes the controlling material parameter. Accordingly, the incidence of a tail in the $P_C(d)$ data may be taken as a useful indicator of impending subsurface radial cracking, without the need for onerous sectioning procedures. In the present case, a fracture mechanics treatment of radial cracking in the coating flexure mode would require a full elastic–plastic analysis of the contact stress field in the entire bilayer structure, using finite element or analogous modelling.[25] In this context, the $P_Y(d)$ curve remains a most useful lower bound for radial cracking, with safety factor built in.

It is interesting to compare the present results for porcelain-fused-to-metal bases with analogous porcelain-fused-to-ceramic bases. Ceramics such as alumina can provide relatively rigid supports for porcelain and other brittle coating systems,[26] and are currently in use as core materials for all-ceramic crowns in dentistry.[1] As indicated in the preceding paper,[10] a stiffer ceramic substrate can depress P_C values even lower than those for the stiffest metals. On the other hand, such ceramics are much harder, and thus not so prone to yield. In principle, therefore, we may expect ceramic substrates to provide superior supports for brittle coatings. This has implications in the context of dental crown design. On the other hand, it should be remembered that dental crowns are bonded to comparatively soft tooth dentin, so that the structures are strictly trilayers rather than bilayers. Under such conditions the support ceramic layer may itself undergo significant flexure on the compliant support, and may therefore itself be subject to fracture.[27] In such cases the yield properties of the metal interlayers need to be balanced against the strength properties of the ceramic interlayers.

Finally, we acknowledge limitations in the present study. A complete description of the radial crack system would require detailed analysis of the tensile stresses in the coating undersurface. As mentioned above, this would require a detailed nonlinear elastic–plastic analysis. Equations (2) and(3) are bounding relations, applicable in the limit of ideally small contacts ($r \ll d$)—in reality, the $P_Y(d)$ functions in Figs. 3–5 will lie above the solid curves plotted, dependent on r. We have avoided consideration of residual stresses in the coating, by matching thermal expansion coefficients between porcelain and metal. In certain systems such residual compression stresses could act to inhibit fracture in the coating layers (provided the bilayer preparation process is not compromised). Also, we have observed no delamination in our experiments. However, delamination could be a factor in extreme cases, at high contact loads or in cyclic loading, where the metal substrate undergoes enough deformation to open up an interfacial fracture on releasing the contact load.[10,28]

ACKNOWLEDGMENTS

The authors thank D. Castaldini at Perth Dental Hospital and P. Chantler at the School of Oral Health Science, The University of Western Australia, for assistance in preparing the porcelain/alloy specimens, and to B.T. Latella for the elastic modulus determinations in Table I. This work was supported by grants from the Australian Research Council and the United States National Institute of Dental Research.

REFERENCES

1. J.R. Kelly, Ann. Rev. Mater. Sci. **27,** 443 (1997).
2. J.R. Kelly, J. Prosthet. Dent. **81,** 652 (1999).
3. J.C. Knight, T.F. Page, and I.M. Hutchings, Thin Solid Films **177,** 117 (1989).
4. K. Komvopolous, ASME J. Tribology **111,** 430 (1989).
5. M.V. Swain and J. Mencik, Thin Solid Films **253,** 204 (1994).
6. D.F. Diao, K. Kato, and K. Hokkirigawa, Trans. ASME J. Tribology **116,** 860 (1994).
7. Y. Sun, A. Bloyce and T. Bell, Thin Solid Films **271,** 122 (1995).
8. L. An, H.M. Chan, N.P. Padture, and B.R. Lawn, J. Mater. Res. **11,** 204 (1996).
9. A.C. Fischer-Cripps, B.R. Lawn, A. Pajares, and L. Wei, J. Am. Ceram. Soc. **79,** 2619 (1996).
10. H. Zhao, X.Z. Hu, M.B. Bush, and B.R. Lawn, J. Mater. Res. **15,** 676 (2000).
11. H. Chai, B.R. Lawn, and S. Wuttiphan, J. Mater. Res. **14,** 3805 (1999).

12. D. Tabor, Hardness of Metals (Clarendon, Oxford, U.K. 1951).
13. O. Prakash, P. Sarkar, and P.S. Nicholson, J. Am. Ceram. Soc. **78,** 1125 (1995).
14. H. Wang and X.Z. Hu, J. Am. Ceram. Soc. **79,** 553 (1996).
15. I.M. Peterson, A. Pajares, B.R. Lawn, V.P. Thompson, and E.D. Rekow, J. Dent. Res. **77,** 589 (1998).
16. F. Guiberteau, N.P. Padture, and B.R. Lawn, J. Am. Ceram. Soc. **77,** 1825 (1994).
17. H. Cai, M.A. Stevens Kalceff, and B.R. Lawn, J. Mater. Res. **9,** 762 (1994).
18. N. Schwarzer, F. Richter, and G. Hecht, Surf. Coat. Technol. **114,** 292 (1999).
19. K.L. Johnson, Contact Mechanics (Cambridge University Press, London, U.K. 1985).
20. B.R. Lawn, J. Am. Ceram. Soc. **81,** 1977 (1998).
21. F.C. Frank and B.R. Lawn, Proc. Roy. Soc. Lond. A **299,** 291 (1967).
22. B.R. Lawn and T.R. Wilshaw, J. Mater. Sci. **10,** 1049 (1975).
23. S. Timoshenko and J.N. Goodier, Theory of Elasticity (McGraw-Hill, New York, 1951), Ch. 8.
24. H. Chai and B.R. Lawn, J. Mater. Res. **15,** 1017 (2000).
25. B.R. Lawn, K.S. Lee, H. Chai, A. Pajares, D.K. Kim, S. Wuttiphan, I.M. Peterson, and X. Hu, Advanced Engineering Materials **2,** 745 (2000).
26. S. Wuttiphan, Ph.D. Thesis, University of Maryland, College Park, MD, 1997.
27. P. Miranda, A. Pajares, F. Guiberteau, F.L. Cumbrera, and B.R. Lawn, J. Mater. Res. **16,** 115 (2001).
28. A. Pajares, L. Wei, B.R. Lawn, and C.C. Berndt, J. Am. Ceram. Soc. **79,** 1907 (1996).